

SIL1 improves cognitive impairment in APP23/PS45 mice by regulating amyloid precursor protein processing and A β generation

Qunxian Wang¹, Yanshuang Jiang¹, Zijun Meng¹, Xiangjun Dong¹, Dongjie Hu¹, Liangye Ji¹, Weihui Zhou^{1,*}, Weihong Song^{1,2,3,*}

¹ Chongqing Key Laboratory of Child Neurodevelopment and Cognitive Disorders, Ministry of Education Key Laboratory of Child Development and Disorders, National Clinical Research Center for Child Health and Disorders, China International Science and Technology Cooperation Base of Child Development and Critical Disorders, Children's Hospital of Chongqing Medical University, Chongqing 400000, China

² Second Affiliated Hospital and Yuying Children's Hospital, Institute of Aging, Key Laboratory of Alzheimer's Disease of Zhejiang Province, Wenzhou Medical University, Wenzhou, Zhejiang 325000, China

³ Oujiang Laboratory (Zhejiang Lab for Regenerative Medicine, Vision and Brain Health), Wenzhou, Zhejiang 325001, China

ABSTRACT

SIL1, an endoplasmic reticulum (ER)-resident protein, is reported to play a protective role in Alzheimer's disease (AD). However, the effect of SIL1 on amyloid precursor protein (APP) processing remains unclear. In this study, the role of SIL1 in APP processing was explored both *in vitro* and *in vivo*. In the *in vitro* experiment, SIL1 was either overexpressed or knocked down in cells stably expressing the human Swedish mutant APP695. In the *in vivo* experiment, AAV-SIL1-EGFP or AAV-EGFP was microinjected into APP23/PS45 mice and their wild-type littermates. Western blotting (WB), immunohistochemistry, RNA sequencing (RNA-seq), and behavioral experiments were performed to evaluate the relevant parameters. Results indicated that SIL1 expression decreased in APP23/PS45 mice. Overexpression of SIL1 significantly decreased the protein levels of APP, presenilin-1 (PS1), and C-terminal fragments (CTFs) of APP *in vivo* and *in vitro*. Conversely, knockdown of SIL1 increased the protein levels of APP, β -site APP cleavage enzyme 1 (BACE1), PS1, and CTFS, as well as APP mRNA expression in 2EB2 cells. Furthermore, SIL1 overexpression reduced the number of senile plaques in APP23/PS45 mice. Importantly, Y-maze and Morris Water maze tests demonstrated that SIL1 overexpression improved cognitive impairment in APP23/PS45 mice. These findings indicate that SIL1 improves cognitive impairment in APP23/PS45 mice by inhibiting APP amyloidogenic processing and

suggest that SIL1 is a potential therapeutic target for AD by modulating APP processing.

Keywords: Alzheimer's disease; SIL1; APP processing; Cognitive impairment

INTRODUCTION

Alzheimer's disease (AD) is the leading cause of dementia in older adults, characterized by progressive learning and memory impairment. Pathological hallmarks of AD include extracellular senile plaques and intracellular neurofibrillary tangles, generated from hyperphosphorylated tau and neuronal or synaptic loss (Liao et al., 2020; Peng et al., 2022). The primary component of senile plaques is the β -amyloid peptide (A β), derived from amyloid precursor protein (APP) through sequential cleavage of β -secretase (BACE1) and γ -secretase in the amyloidogenic pathway (Ly et al., 2013; Zhang et al., 2017, 2020). APP, a single transmembrane protein, matures in the endoplasmic reticulum (ER) and Golgi apparatus before localizing to the plasma membrane (O'Brien & Wong, 2011). APP exists in three main isoforms: the 695-amino acid isoform, which is expressed predominantly in the central nervous system, and the 751- and 770-amino acid isoforms, which are ubiquitously expressed (Bayer et al., 1999). Under physiological conditions, APP is primarily cleaved within the A β domain at the leu¹⁷ site by α -secretase, generating secreted sAPP α and C83 (CTF α 83) (Esch et al., 1990), at the Glu¹¹ β -secretase site by BACE1, generating C89 (CTF) (Zhang et al., 2017), or at the Phe²⁰ θ -site by BACE2, generating C80 (Wang et al., 2019), leading to a nonamyloidogenic pathway. However, under pathological

This is an open-access article distributed under the terms of the Creative Commons Attribution Non-Commercial License (<http://creativecommons.org/licenses/by-nc/4.0/>), which permits unrestricted non-commercial use, distribution, and reproduction in any medium, provided the original work is properly cited.

Copyright ©2024 Editorial Office of Zoological Research, Kunming Institute of Zoology, Chinese Academy of Sciences

Received: 24 February 2024; Accepted: 07 April 2024; Online: 08 April 2024

Foundation items: The work was supported by the National Natural Science Foundation of China (82230043, 82293642)

*Corresponding authors, E-mail: zwh@hospital.cqmu.edu.cn; weihong@wmu.edu.cn

conditions, APP is initially cleaved by BACE1 at the Asp¹ site, generating secreted sAPP β and C99 (CTF β 99), with C99 further cleaved by γ -secretase to generate CTF β and A β (Deng et al., 2013; Zhang et al., 2017), leading to an amyloidogenic pathway. Early pathological deposition of A β in AD is believed to be a fundamental driver of AD pathology, promoting other disorders such as tau pathology (Karran & De Strooper, 2022; Selkoe & Hardy, 2016; Zhang et al., 2023b).

SIL1 nucleotide exchange factor (SIL1) is an ER-resident protein encoded by the *SIL1* gene located on chromosome 5q31.2. It functions as an adenine nucleotide exchange factor for Bip, a member of the heat shock protein 70 family, and acts as a co-chaperone of Bip by regulating its ATPase activity and facilitating the release of substrate proteins (Chung et al., 2002; Rosam et al., 2018). In 2005, SIL1 was identified by two independent research groups as the leading cause of Marinesco-Sjögren syndrome (MSS; OMIM 248800), a rare multisystem disorder in early infants (Anttonen et al., 2005; Senderek et al., 2005). Loss-of-function mutations in SIL1 disrupt the interaction between SIL1 and Bip, leading to abnormal cortical development, considered an important factor contributing to mental retardation in MSS (Inaguma et al., 2014). Additionally, SIL1 is also thought to play a role in neurodevelopment and learning through mechanisms independent of its interaction with Bip (Labisch et al., 2018; Xu et al., 2019).

Previous studies have demonstrated increased SIL1 levels in surviving neurons of patients with AD and noted alterations in the expression of proteins implicated in neurodegeneration (Labisch et al., 2018). SIL1 has also been shown to mitigate tau hyperphosphorylation associated with elevated Bip levels (Liu et al., 2016), suggesting a potential protective role in AD. Additionally, evidence indicates that SIL1 may exert beneficial effects in other neurodegenerative diseases, such as amyotrophic lateral sclerosis (ALS) (Filézac De L'Étang et al., 2015). However, whether SIL1 affects APP processing, a critical factor in AD pathology, remains unclear. To address this, the classical APP23/PS45 mouse model and cells stably transfected with the Swedish mutant APP were used to investigate the effects of SIL1 on APP processing.

MATERIALS AND METHODS

Animals

APP23/PS45 model mice were used as they produce visible senile plaques by 1.5 months of age and experience exacerbated deposition with age. The APP23/PS45 transgenic mice (provided by Novartis) were generated by crossing APP23 mice carrying the Swedish APP751(KM \rightarrow NL) mutant transgene with PS45 mice overexpressing the human G384A mutated presenilin-1 (PS1). The mice were housed at the Children's Hospital of Chongqing Medical University Animal Care Centre under a 12 h light-dark cycle (lights on from 0700h to 1900h), with free access to food and water, in a temperature- and humidity-controlled individual ventilation cage (IVC) room. Genotypes were confirmed by polymerase chain reaction (PCR) using DNA extracted from tail tissues. All animal experiments were performed in accordance with the Guide for the Care and Use of Laboratory Animals of the Ethics Committee of Chongqing Medical University. All experimental protocols were approved by the Animal Study Committee of the Children's Hospital of Chongqing Medical University (approval number CHCMU-IACUC20221227006).

Plasmids and siRNA

Myc-his-tagged pcDNA4 was used as the backbone to construct SIL1-myc plasmids. The cDNA extracted from HEK293 cells was used as an amplification template for PCR. Primers were synthesized by Tsingke Biotechnology (Beijing, China), with the following sequences: (forward) 5'-TTGGTACCGAGCTCGGATCCGCCACCATGGCTCCCCAGAGCCTGC-3'; (reverse) 5'-GAAGGGCCCTCTAGACTCGAGTCTCAGCTCCTTCAGCAAGCTGTTGACAG-3'. For SIL1 knockdown *in vitro*, small interfering RNA (siRNA) targeting human SIL1 and negative RNA (siNC) were synthesized by WZ Bioscience (China). The target sequences for SIL1 siRNA were: (sense) 5'-GCUGCGCUCUUGAUCUUGAATT-3'; (anti-sense) 5'-UACAAGAUCAAAGAGCGCAGCTT-3'.

Cell culture and transfection

All cell lines were cultured in 90% Dulbecco's modified Eagle medium (DMEM) (Cat#C11995500BT, Gibco, USA) supplemented with 10% fetal bovine serum (FBS) (Cat#10270-106, Gibco, USA) and maintained in an incubator at 37°C with 5% CO₂. The N2A^{APP} cell line (Du et al., 2019), consisting of mouse neuroblastoma (N2A) cells stably expressing human Swedish mutant APP695, was cultured in 90% DMEM supplemented with 10% FBS containing 50 μ g/mL G418 (Cat#11811031, Gibco, USA). The 2EB2 cell line (Sun et al., 2005), comprising human embryonic kidney (HEK293) cells stably expressing human Swedish mutant APP695 and human BACE1, was maintained in 90% DMEM supplemented with 10% FBS containing 100 μ g/mL zeocin (Cat#R25001, Invitrogen, USA) and 50 μ g/mL G418 (Cat#11811031, Gibco, USA). The N2A^{APP} and 2EB2 cells are not listed as commonly misidentified cell lines by the International Cell Line Authentication Committee. Authentication of the cell lines after treatment was performed by western blotting to confirm overexpressing bands. The maximum number of passages for each cell line was less than 50. Plasmids and siRNAs were transfected into the cells using Lipofectamine 2000 (Cat#11668019, Thermo Fisher Scientific, USA) according to the manufacturer's protocols.

Adeno-associated virus and microinjection

The GV388 plasmid was used as a backbone for overexpressing SIL1 *in vivo*, with the following primers used to construct the SIL1-containing plasmid: (forward) 5'-GGAGGTAGTGAATGGATCCCGCCACCATGGCTCCCCAGAGCCTGCC-3'; (reverse) 5'-TCACCATGGTGGCGGGATCAGGGCCGGGATTCTCTCCACGTCACCGCCTGCTTCAGCAGG-3'. The constructed plasmid was then transferred to an adeno-associated virus (AAV) to create AAV-SIL1-EGFP (Genechem Co., Ltd., Shanghai, China). The titer of AAV-SIL1-EGFP was 9.53E+12 vg/mL. Mice (6 weeks old, weighing 16–18 g) were anesthetized with an intraperitoneal (i.p.) injection of sodium pentobarbital (60 mg/kg) to minimize suffering during the procedure. Core temperature was maintained at 36.5 \pm 0.5°C. The scalp was shaved with clippers and disinfected with iodine before being mounted on a stereotaxic instrument. After the scalp was incised to expose the skull, 1 μ L of AAV-SIL1-EGFP or AAV-EGFP was microinjected into each lateral ventricle via drilled holes (0.5 mm posterior, \pm 1.1 mm lateral, and 3 mm ventral relative to bregma). The scalp was then sutured with absorbable sutures.

After the operation, the mice were carefully relocated to a 37°C incubator to maintain their core temperature. Once they regained consciousness, they were gently transferred back to

their newly prepared cages filled with soft, clean padding. Throughout this period, their vital signs were monitored to ensure their well-being. No additional analgesics were administered to minimize the risk of adverse reactions during short-term repeated administration, prioritizing the safety and well-being of the mice. Sodium pentobarbital was chosen due to its simplicity, convenience, low cost, effectiveness, rapid induction of anesthesia, broad safe dosage range, and minimal risk of mortality and reflexes during surgery. This study was not pre-registered, and no randomization or blinding was performed. No exclusion criteria were predetermined, and no animals were excluded. Given the high mortality rate of APP23/PS45 mice, we initially microinjected negative-control AAV into 10 wild-type (WT) mice (five females and five males) and 24 APP23/PS45 mice (10 males and 14 females). Subsequently, we microinjected SIL1-containing AAV into 25 APP23/PS45 mice (10 males and 15 females).

The sample size decided for each experiment was based on our previous study (Zhang et al., 2020). All animals received AAV microinjections at 6 weeks of age, and all remaining living mice underwent behavioral tests at 5 months of age, prior to sacrifice. The mice were anesthetized with urethane (Cat#U2500, Sigma, USA; 0.8 mL/20 g, i.p.) using a 2.5 mL injection syringe. Thereafter, they received cardiac perfusion with physiological saline after complete anesthesia for subsequent extraction of brain tissues.

Western blotting

Cells and brain tissues of the mice were collected in RIPA lysis solution containing a protease inhibitor (Cat#4693159001, Roche, Switzerland) for 30 min. The samples were then centrifuged at 14 000 r/min for 15 min at 4°C. All supernatants were transferred to new tubes. A BCA kit (Cat#23227, Thermo Fisher Scientific, USA) was used to detect the concentration of proteins according to the manufacturer's protocols. Protein samples (30–60 µg) were diluted with 5× sample buffer and boiled at 95°C for 8 min. The samples were then separated on 12.5% tris-glycine sodium dodecyl sulfate-polyacrylamide gel electrophoresis (SDS-PAGE) or 16% tris-tricine SDS-PAGE and transferred onto well-cut, 0.22 µm aperture polyvinylidene fluoride (PVDF) membranes (CAT#SLGVR33RB, Millipore, USA). The membranes were then blocked in 5% skim milk or 5% bovine serum albumin for 1.5 h.

Aβ WB was performed following previously published methods (Liu et al., 2022). Briefly, lysates were separated on 16% tricine gel, followed by electro-transfer. The membranes were then twice boiled in phosphate-buffered saline (PBS) in a microwave for 3 min, and subsequently cooled to room temperature. The membranes were blocked in PBS containing 0.1% Tween-20 and 5% bovine serum albumin and immunoblotted with indicated primary antibodies overnight at 4°C. After incubation with goat anti-rabbit immunoglobulin G (IgG) (Cat#A0208, Beyotime, China) or anti-mouse IgG (Cat#A0216, Beyotime, China) at room temperature for 1.5 h, the proteins were detected using a Bio-Rad Imager and an ECL WB substrate (Cat#170-5061, Bio-Rad, USA). Primary antibodies SIL1 (Cat#ab228868, Abcam, UK, 1:1 000), PS1 (Cat# ab15458, Abcam, UK, 1:1 000), and BACE1 (Cat#ab108394, Abcam, UK, 1:1 000) were used to detect the SIL1, PS1, and BACE1 bands, respectively. A C20 (1:1 000–3 000) polyclonal antibody produced in our laboratory was used to detect the C-terminal fragments of APP (Zheng

et al., 2022). The 6E10 antibody (Cat#SIG-39240, BioLegend, USA, 1:10 000) targeting the N-terminal of Aβ was used to detect soluble APP fragments (sAPPα and Aβ). The GAPDH (Cat#60004-1-Ig, Proteintech, China, 1:50 000–500 000), actin (Cat#ac026, ABclonal, China, 1:100 000), and tubulin (Cat#66031-1-Ig, Proteintech, China, 1:20 000–100 000) antibodies were used to detect GAPDH, actin, and tubulin bands, respectively.

RNA sequencing (RNA-seq)

To explore the mechanism by which SIL1 influences APP processing, total RNA was extracted from 2EB2 cells in the siRNA and siNC groups using TRIzol (Cat#15596026, Invitrogen, USA). All samples were tested using the Illumina NovaSeq 6000 platform with the PE150 pattern at the LianChuan Company (Zhejiang, China). All raw sequence data reported in this paper were deposited in the Genome Sequence Archive (Genomics, Proteomics & Bioinformatics 2021) at the National Genomics Data Center (Nucleic Acids Res 2022), China National Center for Bioinformation/Beijing Institute of Genomics, Chinese Academy of Sciences (GSA-Human: HRA005214) and are publicly accessible at <https://ngdc.cnpc.ac.cn/gsa-human>. The data were also deposited in the NCBI database (BioProject PRJNA1099875) and Science Data Bank database (DOI: 10.57760/sciencedb.j00139.00131). The researchers conducting the experiments were blinded to the study groups.

Cycloheximide (CHX) treatment

To determine the effect of SIL1 on APP degradation, 2EB2 cells were transfected with siRNA or siNC for 48 h, then seeded into 12-well plates with six wells per group. The cells were subsequently treated with 100 µg/mL CHX (Cat#C8030-100, Solarbio, China) and collected at 0, 1, 2, 4, 8, and 12 h for WB analysis.

Dactinomycin treatment for RNA stability

To investigate the effect of SIL1 on APP mRNA degradation, 2EB2 cells were transfected with either siRNA or siNC for 48 h, then seeded into 12-well plates with four wells per group. For RNA stability assessment, the cells were treated with 5 µg/mL dactinomycin (Cat#HY-17559, MCE, USA) to inhibit RNA synthesis. The samples were then collected at 0, 1, 2, and 4 h for subsequent RNA extraction using TRIzol reagent (Cat#15596026, Invitrogen, USA), following established protocols. The extracted RNA underwent reverse transcription to generate cDNA using PrimeScript™ RT Master Mix (Cat#RR036A, Takara, Japan), following the manufacturer's procedures. The resulting cDNA was used for quantitative PCR using a SYBR PremixExTq2007 kit (Cat#RR820A, Takara, Japan) according to the manufacturer's instructions. The APP primers for quantitative PCR were: (forward) 5'-TT GTAAGTGATGCCCTTCTCGTT-3'; (reverse) 5'-AGCAACATG CCGTAGTCATGCAA-3'. The GAPDH primers for quantitative PCR were: (forward) 5'-CTCTGCTCCTCTGTTCGAC-3'; (reverse) 5'-GCGCCAATACGACCAATC-3'.

Immunohistochemistry

Half brain sections were fixed in freshly prepared 4% paraformaldehyde in PBS for 4–5 days, then dehydrated in a 30% sucrose solution in PBS for 2 days for sectioning into 30 µm coronal brain slices. The brain slices were washed three times with 0.3% PBST (1 L of 0.01 mol/L PBS added to 3 mL of Triton X-100) (Cat#9002-93-1, Sigma, USA) and incubated with 30% H₂O₂ (Cat#7722-84-1, Sigma, USA) for 30 min at

37°C. The brain slices were blocked with a 10% bovine serum albumin solution for 1 h at room temperature, then incubated with mouse monoclonal 4G8 antibody (Cat#SIG-39240, BioLegend, USA, 1:500) overnight at 4°C. The plaques on the brain slices were assayed using an ABC kit (Cat#PK6102, Vector, USA) and a DAB kit (Cat#SK4105, Vector, USA) and scanned using a full-pick scanner. The number of plaques was counted using ImageJ software.

Immunofluorescent staining

Mouse brain slices (30 μ m thick) were washed three times using 1 \times PBS buffer, each lasting 10 min. Subsequently, the cleaned slices were immersed in an immunofluorescent blocking solution (Cat#P0260, Beyotime, China) for 1 h at room temperature, then incubated with SIL1 (Cat#ab228868, Abcam, UK, 1:1 000) and NeuN (Cat#ab177487, Abcam, UK, 1:1 000) primary antibodies at 4°C. After overnight incubation, the slices were incubated with donkey anti-rabbit (Cat#A11001, Invitrogen, USA, 1:1 000) or anti-mouse IgG (Cat#A11004, Invitrogen, USA, 1:1 000) for 1 h at room temperature. The slices were finally sealed with an anti-fluorescence quenching sealing solution (including DAPI) (Cat#P0131, Beyotime, China) and examined using a laser confocal microscope (Nikon, Japan) to capture immunofluorescence.

Y-maze test

The Y-maze test was employed to assess short-term spatial working memory in mice, as described previously (Kraeuter et al., 2019). Mice were placed at the starting point of the initial arm with their head facing the intersection of the three arms and allowed to explore freely for 8 min. Behavior and activity tracks of the mice were recorded and analyzed using ANY-maze (San Diego Instruments, USA). A successful alteration was defined as three consecutive entries into different arms. The total number of events was defined as the total number of entries into the arms minus two. Spontaneous alterations were determined by the ratio of the number of mice visiting three different arms in a row (number of successful alterations) to the total number of events.

Morris water maze (MWM) test

The MWM test was used to determine spatial memory and learning in mice, as described previously (Bromley-Brits et al., 2011). The test was performed in a circular pool (1.5 m diameter and 0.6 m depth) filled with opaque water. A platform (10 cm diameter) was placed in the southwest (SW), northwest (NW), northeast (NE), center, and southeast (SE) quadrants of the pool, 1 cm above the water on the first day. It was then placed in the SW quadrant 1 cm below the water on the second to fifth days and was removed on the last day. On day one, the mice were trained to find the visible platform within 60 s. On days 2–5, the mice were allowed to freely search for the hidden platform for 60 s. Each mouse underwent five trials daily from four points in the pool with an interval of 1 h. On the last day, the mice were allowed to search for the removed platform for 60 s from the same point in the pool. Behaviors were recorded and analyzed using ANY-maze (San Diego Instruments, USA). The investigators were blinded to the study groups during the experiment and data analysis.

Statistical analysis

All data were analyzed using SPSS v.25. GraphPad Prism was used to create quantification figures. All results are

presented as mean \pm standard error of the mean (SEM). Replicate numbers are indicated in the figure legends. Normality was determined using the Shapiro-Wilk test. Comparisons between two groups were performed using two-tailed Student's *t*-test. Multiple comparisons were analyzed using one-way analysis of variance (ANOVA) or two-way ANOVA with *post hoc* Dunnett's multiple comparisons test. The level of statistical significance was set at $P < 0.05$. No statistical tests for outliers were conducted, and no data points were excluded.

RESULTS

SIL1 protein was significantly decreased in APP23/PS45 mice

Previous reports have suggested that SIL1 plays a protective role in AD. To determine the role of SIL1 in APP23/PS45 mice, WB was used to test the SIL1 protein levels in the brains of APP23/PS45 and age-matched WT mice at different ages. Results showed that SIL1 was significantly decreased in the brains of APP23/PS45 mice compared to the age-matched WT mice at 3 months (APP23/PS45 vs. WT: 0.869 \pm 0.111 vs. 1.292 \pm 0.108, $P = 0.044$, $n = 6-7$, Figure 1A, B) and 6 months of age (APP23/PS45 vs. WT: 0.657 \pm 0.067 vs. 1.407 \pm 0.204, $P = 0.007$, $n = 6$, Figure 1C, D). WB was also used to determine the protein level of APP. Results showed that the APP protein was significantly increased in the AD mice compared to their corresponding age-matched WT mice at 3 months (1.210 \pm 0.055 vs. 0.772 \pm 0.051, $P < 0.001$, $n = 6-7$) and 6 months (1.180 \pm 0.056 vs. 0.838 \pm 0.068, $P = 0.004$, $n = 6$; Figure 1A–D). Immunofluorescence staining was performed to investigate the localization of SIL1 in the brain. Results showed that SIL1 mainly resided in the dentate gyrus (DG), CA1, CA3, and cortical regions in both 5-month-old WT and age-matched APP23/PS45 mice (Figure 1E). Overall, SIL1 protein levels showed a significant decrease in APP23/PS45 mice, similar to previous research (Liu et al., 2016).

Overexpression of SIL1 inhibited APP processing *in vitro*

Given the abnormal expression of SIL1 in APP23/PS45 mice, plasmids containing *SIL1* (*SIL1*-myc) or an empty vector were transfected into N2A^{APP} and 2EB2 cells, respectively, to determine the effects of SIL1 on APP amyloidogenic processing. WB was used to detect the protein levels of SIL1, APP, BACE1, PS1, and APP-CTFs in the APP amyloidogenic pathway. Results showed a significant increase in SIL1 protein levels after transfection of *SIL1*-myc into N2A^{APP} cells (SIL1 vs. vector, 0.77 \pm 0.14 vs. 0.07 \pm 0.003, $P = 0.016$, $n = 4$, Figure 2A, B). Conversely, the protein levels of APP (SIL1 vs. vector, 0.21 \pm 0.04 vs. 0.44 \pm 0.03, $P = 0.004$, $n = 4$, Figure 2A, C), PS1 (SIL1 vs. vector, 1.01 \pm 0.04 vs. 1.34 \pm 0.07, $P = 0.008$, $n = 4$, Figure 2A, E), CTF-99 (SIL1 vs. vector, 0.16 \pm 0.01 vs. 0.35 \pm 0.05, $P = 0.012$, $n = 4$, Figure 2A, F), and CTF-89 (SIL1 vs. vector, 0.17 \pm 0.03 vs. 0.28 \pm 0.04, $P = 0.049$, $n = 4$, Figure 2A, G) showed a significant decrease compared to the vector group, while no significant change was observed in the BACE1 protein level (SIL1 vs. vector, 0.21 \pm 0.04 vs. 0.435 \pm 0.03, $P = 0.719$, $n = 4$, Figure 2A, D).

To further confirm the role of SIL1 in APP processing, SIL1 was overexpressed in 2EB2 cells, followed by WB analysis. Results showed that the SIL1 protein level was markedly elevated after transfection with *SIL1*-myc (SIL1 vs. vector, 1.50 \pm 0.19 vs. 0.01 \pm 0.02, $P < 0.001$, $n = 5$, Figure 2H, I). In

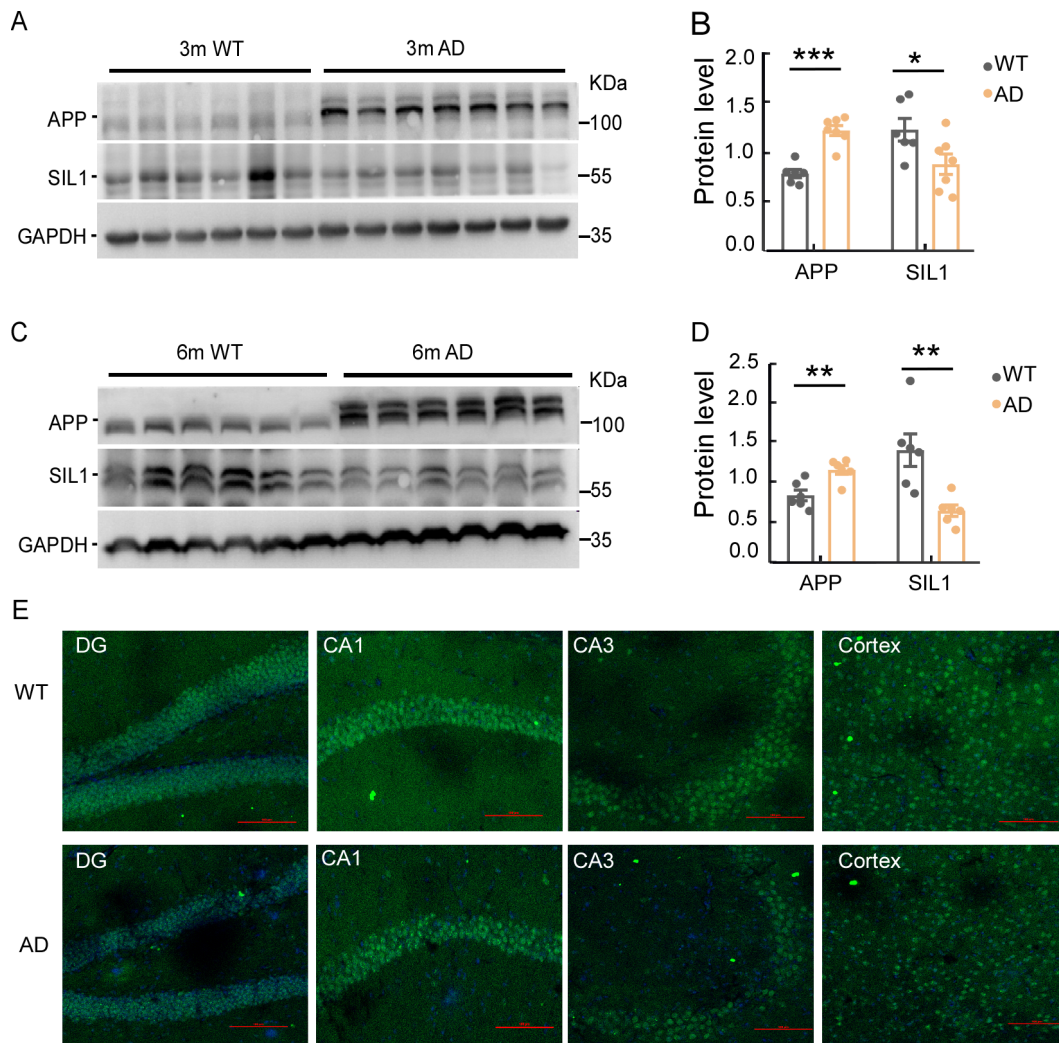


Figure 1 Protein level of SIL1 decreased in APP23/PS45 mice

A, B: Protein levels of SIL1 and APP in the hippocampus of 3-month-old APP23/PS45 mice and age-matched WT mice, with APP and SIL1 levels normalized to GAPDH levels for comparison. $n=6-7$ animals in each group (WT mice, $n=6$; APP23/PS45 mice, $n=7$). C, D: Protein levels of SIL1 and APP in the cortex of 6-month-old APP23/PS45 mice and age-matched WT mice, with APP and SIL1 levels normalized to GAPDH levels for comparison. $n=6$ animals in each group. E: Immunofluorescent staining of SIL1 and DAPI in DG, CA1, CA3, and cortical area of 5-month-old WT mice and age-matched APP23/PS45 mice. Scar bar: 100 μm . Data are presented as mean \pm SEM. P -values were determined by student's t -tests. *: $P<0.05$; **: $P<0.01$; ***: $P<0.001$.

contrast, the protein levels of APP (SIL1 vs. vector, 0.62 ± 0.08 vs. 0.90 ± 0.04 , $P=0.014$, $n=5$, Figure 2H, J), PS1 (SIL1 vs. vector, 0.83 ± 0.04 vs. 1.10 ± 0.10 , $P=0.041$, $n=5$, Figure 2H, L), CTF-99 (SIL1 vs. vector, 0.47 ± 0.05 vs. 0.64 ± 0.02 , $P=0.015$, $n=5$, Figure 2H, M), and CTF-89 (SIL1 vs. vector, 0.52 ± 0.05 vs. 0.72 ± 0.05 , $P=0.029$, $n=5$, Figure 2H, N) were significantly decreased compared to the vector group, while the protein levels of BACE1 were not significantly affected (SIL1 vs. vector, 0.99 ± 0.11 vs. 1.07 ± 0.06 , $P=0.495$, $n=5$, Figure 2H, K). Thus, SIL1 overexpression significantly suppressed APP processing *in vitro*.

Knockdown of SIL1 enhanced APP processing by increasing APP expression *in vitro*

Given that SIL1 expression was decreased in APP23/PS45 mice, and SIL1 overexpression significantly suppressed APP amyloidogenic processing, we further explored the effects of SIL1 on APP amyloidogenic processing using siRNA to target and knockdown SIL1 in 2EB2 cells. Results showed that SIL1 knockdown in 2EB2 cells led to a significant decrease in the protein level of SIL1 (siSIL1 vs. siNC, 0.73 ± 0.07 vs.

1.27 ± 0.15 , $P=0.018$, $n=4$, Figure 3A, B), as well as a significant increase in the protein levels of APP (siSIL1 vs. siNC, 1.11 ± 0.03 vs. 0.89 ± 0.06 , $P=0.021$, $n=4$, Figure 3A, C), PS1 (siSIL1 vs. siNC, 1.14 ± 0.02 vs. 0.86 ± 0.05 , $P=0.002$, $n=4$, Figure 3A, D), BACE1 (siSIL1 vs. siNC, 1.08 ± 0.05 vs. 0.918 ± 0.03 , $P=0.022$, $n=4$, Figure 3A, G), C99 (siSIL1 vs. siNC, 0.63 ± 0.06 vs. 0.39 ± 0.05 , $P=0.023$, $n=4$, Figure 3A, E), and C89 (siSIL1 vs. siNC, 0.60 ± 0.05 vs. 0.37 ± 0.03 , $P=0.01$, $n=4$, Figure 3A, F) compared to the control group. These findings demonstrate that SIL1 knockdown enhanced APP amyloidogenic processing.

To elucidate the effect of SIL1 knockdown on APP amyloidogenic processing, RNA-seq was performed to identify differentially expressed genes (DEGs) after SIL1 knockdown in 2EB2 cells. Genes exhibiting a $\log_2(\text{fold-change})$ exceeding 0.5 were categorized as DEGs. Results indicated that multiple genes were altered following SIL1 knockdown, including down-regulated genes such as *TEME245*, *TMEM109*, *RNF11*, *EIF4G2*, *EFTUD2*, and *SIL1*, and up-regulated genes such as *TPM4*, *NACC1*, *PPP1R14B*, *APP*, *KIF1C*, and *VIM*. The *SIL1*

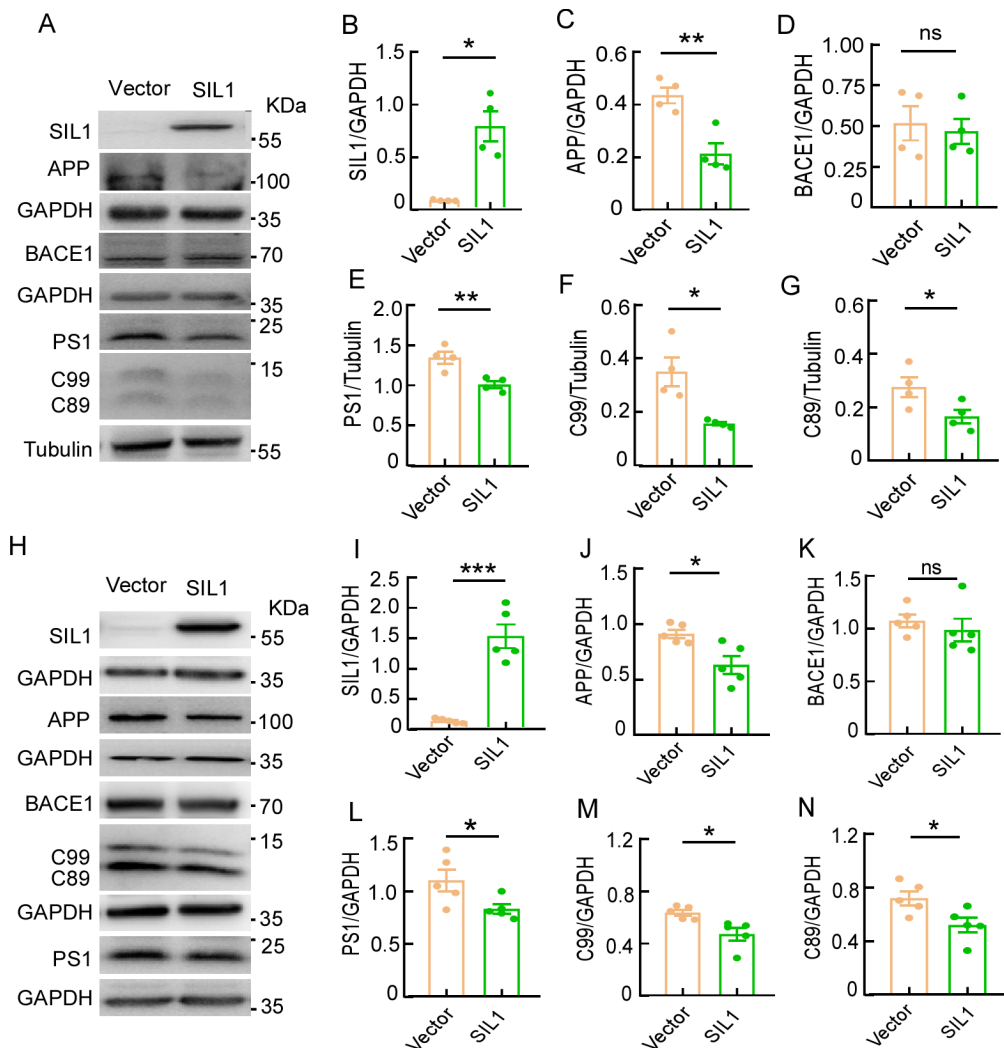


Figure 2 Overexpression of SIL1 significantly reduced APP processing in N2A^{APP} and 2EB2 cells

A: SIL1 overexpression significantly reduced APP processing in N2A^{APP} cells. N2A^{APP} cells were transfected with SIL1-myc plasmids or empty vector, then harvested for western blot analysis after transfection for 24 h. A, C: APP, A, E: PS1, A, F: C99, and A, G: C89 were decreased in the SIL1 overexpression group compared to the empty vector group, with APP, PS1, C99, and C89 levels normalized to their corresponding GAPDH levels for comparison. A, D: BACE1 showed no significant change between SIL1 overexpression and empty vector, with BACE1 levels normalized to GAPDH levels for comparison. $n=4$ of independent cell culture preparations. H: SIL1 overexpression significantly reduced APP processing in 2EB2 cells. 2EB2 cells were also transfected with SIL1-myc plasmids and empty vector, followed by western blot analysis after 24 h of transfection. H, J: APP, H, L: PS1, H, M: C99, and H, N: C89 were significantly decreased in SIL1 overexpression group compared to empty vector group, with APP, PS1, C99, and C89 levels normalized to their corresponding GAPDH or tubulin levels for comparison. H, K: BACE1 showed no significant change between the two groups, with BACE1 levels normalized to GAPDH levels for comparison. $n=5$ of independent cell culture preparations. Data are presented as mean \pm SEM. P -values were determined by student's t -tests. ns: Not significant; * $P<0.05$; ** $P<0.01$.

gene was significantly down-regulated, with SIL1 read counts significantly decreased in the siSIL1 group compared to the siNC group ($P=0.003$, $n=3$, Figure 3H, I). The read count, typically calculated based on original sequencing data (FASTQ files) by comparing reads to the reference genome or transcriptome, represents the number of reads per gene in the sample; that is, the number of sequenced reads mapped to each gene in the sequencing data, directly measuring gene expression and reflecting gene abundance. Simultaneously, the *APP* gene was significantly up-regulated, with APP read counts significantly increased in the siSIL1 group compared to the siNC group ($P=0.001$, $n=3$, Figure 3H, J), also normalized to the reference genome. Furthermore, changes in expression extended to genes associated with membrane integrity, transcriptional regulation processes, and other physiological functions. This complex web of gene expression changes

strongly suggests that SIL1 knockdown enhanced APP amyloidogenic processing by influencing APP transcriptional regulation.

Next, to determine the effect of SIL1 on APP protein degradation, 2EB2 cells were treated with 100 μ g/mL CHX after transfection with siSIL1 or siNC for 48 h. The cells were then collected at 0, 1, 2, 4, 8, and 12 h for WB analysis. Results showed that SIL1 did not affect APP protein degradation ($P>0.05$, $n=5$, Figure 3K, L).

To further determine the effect of SIL1 on the APP mRNA level, 2EB2 cells were treated with 5 μ g/mL dactinomycin to inhibit RNA synthesis after transfection with siSIL1 or siNC for 48 h. The cells were collected at 0, 1, 2, and 4 h for quantitative PCR analysis. Results demonstrated that after SIL1 knockdown, the degradation rate of APP mRNA did not change significantly ($P=0.258$, $n=6$, Figure 3M). These

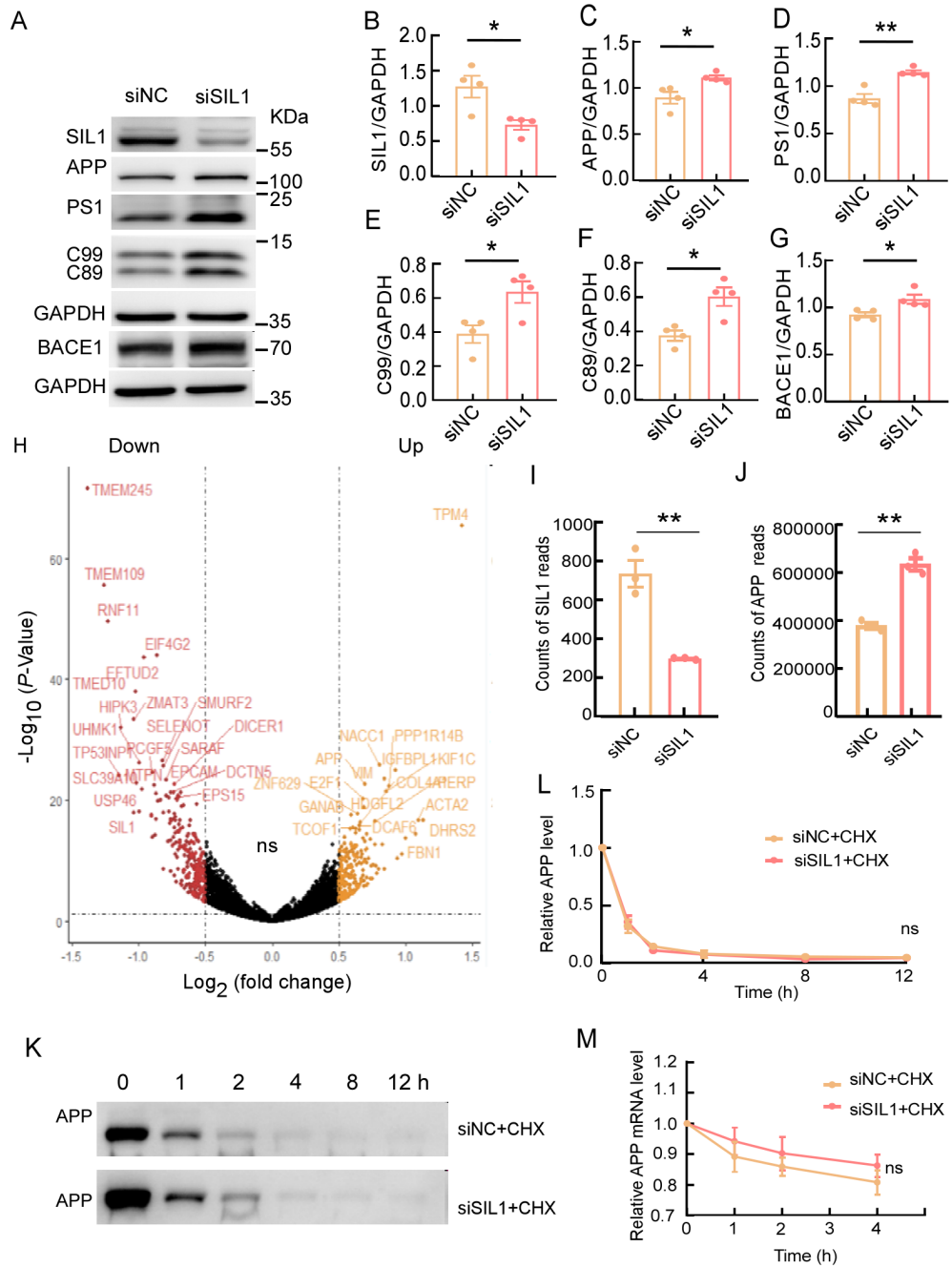


Figure 3 Knockdown of SIL1 increased APP processing in 2EB2 cells

A: WB was used to determine effects of SIL1 knockdown on APP processing in 2EB2 cells. 2EB2 cells were transfected with siRNA to knockdown SIL1 (siSIL1) or negative siRNA (siNC), then harvested for western blot analysis after transfection for 48 h. Protein levels of A, B: APP, A, D: PS1, A, E: C99, A, F: C89, and A, G: BACE1 were significantly increased in the siSIL1 group compared to the siNC group, with protein levels normalized to their corresponding GAPDH levels for comparison. $n=4$ of independent cell culture preparations. H: Volcanic map of differentially expressed genes in 2EB2 cells after transfection with siSIL1 and siNC, as determined using RNA-seq. SIL1 was down-regulated, and APP gene was up-regulated. I, J: Relative qualification of mRNA expression level of SIL1 and APP in 2EB2 cells after transfection with siSIL1 and siNC, with counts of SIL1 and APP reads normalized to the reference genome. $n=3$ of independent cell culture preparations. K, L: APP protein level after treatment with CHX at 0, 1, 2, 4, 8, and 12 h, with APP levels at 1, 2, 4, 8, and 12 h normalized to APP levels at 0 h. $n=5$ of independent cell culture preparations. M: APP mRNA level after treatment with dactinomycin at 0, 1, 2, and 4 h, with APP mRNA levels normalized to GAPDH mRNA levels. $n=6$ of independent cell culture preparations. Data are presented as mean \pm SEM. P -values were determined using student's t -tests in (B–G, I, J) and two-way ANOVA with Dunnett's *post hoc* analysis in (M, L). ns: Not significant; *: $P<0.05$; **: $P<0.01$; ***: $P<0.001$.

findings suggest that SIL1 knockdown in 2EB2 cells may affect transcription regulation but not post-transcriptional gene regulation.

In summary, our results suggest that SIL1 knockdown enhanced APP amyloidogenic processing, likely by regulating

transcription under pathological conditions.

Overexpression of SIL1 improved cognitive impairments in APP23/PS45 mice

As SIL1 was significantly decreased in APP23/PS45 mice, and SIL1 overexpression *in vitro* significantly suppressed APP

processing, we next assessed whether the elevation of SIL1 would improve APP23/PS45 mouse behavior. Firstly, AAV carrying SIL1-cDNA and control AAV were microinjected into the lateral ventricle of mice at 1.5 months of age. After microinjection for 3 months, all living mice underwent the Y-maze test. Results showed that AD-EGFP mice (APP23/PS45 mice microinjected with control AAV) had a lower autonomic alteration rate than WT-EGFP mice (WT mice microinjected with control AAV) ($P=0.013$, $n=10-17$, Figure 4B), suggesting that APP23/PS45 mice had short-term memory impairment. The overexpression of SIL1 significantly increased the autonomic alteration rate in APP23/PS45 mice (AD-SIL1-EGFP, APP23/PS45 mice microinjected with SIL1 AAV) (AD-SIL1-EGFP vs. AD-EGFP, $P=0.009$, $n=17-20$, Figure 4B). This suggests that SIL1 overexpression rescued short-term memory impairment in AD mice.

The MWM test was also applied to determine impacts on spatial learning and memory in mice. Results showed that AD-

EGFP mice had a similar escape latency ($P=0.085$, $n=10-17$, Figure 4D) and swimming distance as WT-EGFP mice ($P=0.670$, $n=10-17$ Figure 4E) on the visible platform day (first day). Moreover, AD mice infected with SIL1-AAV (AD-SIL1-EGFP) showed a similar escape latency ($P=0.452$, $n=17-20$, Figure 4D) and swimming distance ($P=0.925$, $n=17-20$, Figure 4E) as AD-EGFP mice on the visible platform day. These findings suggest that SIL1 elevation did not affect the visual and motor abilities of AD mice. Results also demonstrated that AD-EGFP mice had a significantly longer escape latency on the hidden platform days compared to WT-EGFP mice ($P=0.008$, $n=10-17$, Figure 4F). AD-SIL1-EGFP mice showed a shorter escape latency than AD-EGFP mice, but no significant differences were observed ($P=0.081$, $n=17-20$, Figure 4F). On the final day, AD-EGFP mice spent significantly shorter time crossing the platform zone in the targeted quadrant compared to WT-EGFP mice ($P=0.001$, $n=10-17$, Figure 4G). Moreover, mice overexpressing SIL1

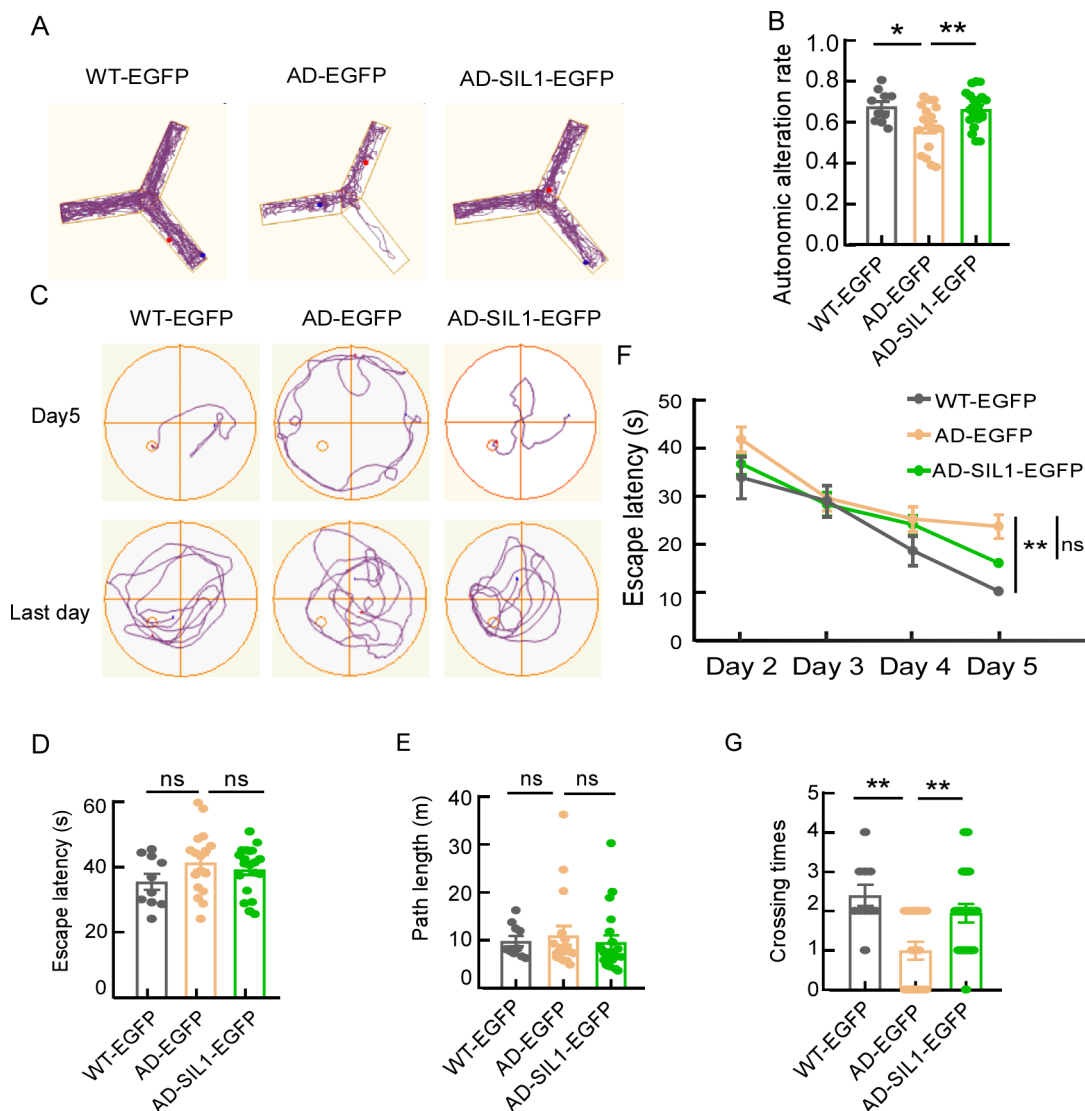


Figure 4 Overexpression of SIL1 improved learning and memory in APP23/PS45 mice

A: Activity tracks of mice in the Y-maze test. B: Spontaneous alteration rate of mice was detected by the Y-maze test. C: Activity track of mice on day 5 and final day in the MWM test. D: Escape latencies of mice on visible platform. E: Path distance of mice on visible platform. F: Escape latencies of mice on hidden platform. G: Time crossing the platform located in target quadrant. $n=10-20$ animals in each group (WT-EGFP, $n=10$; AD-EGFP, $n=17$; AD-SIL1-EGFP, $n=20$). Data are presented as mean \pm SEM. P -values were determined by one-way ANOVA with Dunnett's *post hoc* analysis in B, D, E, G and by two-way ANOVA with Dunnett's *post hoc* analysis in F. ns: Not significant, *: $P<0.05$; **: $P<0.01$.

(AD-SIL1-EGFP) spent significantly longer time crossing the platform zone in the targeted quadrant compared to AD-EGFP mice ($P=0.005$, $n=17-20$, Figure 4G). These findings suggest that SIL1 overexpression significantly rescued spatial memory in AD mice.

Overexpression of SIL1 significantly decreased APP processing *in vivo*

To determine whether SIL1 overexpression improved cognitive impairment in APP23/PS45 mice by inhibiting APP amyloidogenic processing, WB was performed to determine the protein levels of SIL1, APP, BACE1, PS1, CTFs, sAPP α , and A β . Results showed that the protein level of SIL1 was significantly decreased in AD-EGFP mice (0.40 ± 0.04 vs. 0.58 ± 0.05 , $P=0.032$, $n=4$, Figure 5A, B), while the protein levels of APP (1.38 ± 0.09 vs. 0.67 ± 0.02 , $P<0.001$, $n=4$, Figure 5A, C), PS1 (1.41 ± 0.09 vs. 0.92 ± 0.05 , $P<0.001$, $n=4$, Figure 5A, D), C99 (0.84 ± 0.04 vs. 0.00 ± 0.00 , $P<0.001$, $n=4$, Figure 5A, E), C89 (0.92 ± 0.04 vs. 0.00 ± 0.00 , $P<0.001$, $n=4$, Figure 5A, F), BACE1 (2.33 ± 0.32 vs. 0.97 ± 0.15 , $P=0.024$, $n=4$, Figure 5A, G), sAPP α (1.39 ± 0.07 vs. 0.44 ± 0.01 , $P<0.001$, $n=4$, Figure 5A, H), and A β (1.36 ± 0.03 vs. 0.00 ± 0.00 , $P<0.001$, $n=4$, Figure 5A, I) were significantly increased in AD-EGFP mice compared to WT-EGFP mice. After overexpressing SIL1 (AD-SIL1-EGFP) in AD mice, the protein level of SIL1 was significantly increased (0.87 ± 0.05 vs. 0.40 ± 0.04 , $P=0.002$, $n=4-5$, Figure 5A, B), while the protein levels of APP (1.00 ± 0.04 vs. 1.38 ± 0.09 , $P=0.002$, $n=4-5$, Figure 5A, C), PS1 (0.77 ± 0.05 vs. 1.41 ± 0.09 , $P<0.001$, $n=4-5$, Figure 5A, D), C99 (0.41 ± 0.02 vs. 0.84 ± 0.04 , $P<0.001$, $n=4-5$, Figure 5A, E), C89 (0.47 ± 0.03 vs. 0.92 ± 0.04 , $P<0.001$, $n=4-5$, Figure 5A, F), sAPP α (1.08 ± 0.23 vs. 1.39 ± 0.07 , $P=0.02$, $n=4-5$, Figure 5A, H), and A β (1.22 ± 0.06 vs. 1.36 ± 0.03 , $P=0.046$, $n=4-5$, Figure 5A, I) were significantly decreased. The protein level of BACE1 (1.66 ± 0.43 vs. 2.33 ± 0.32 , $P=0.263$, $n=4-5$, Figure 5A, G) showed a non-significant decreasing trend. The WB results suggest that SIL1 overexpression significantly decreased APP amyloidogenic processing *in vivo*.

To further determine the effect of SIL1 on APP amyloidogenic processing, immunohistochemical staining was used to assess senile plaque deposition by A β . Results showed that plaque number significantly decreased in AD-SIL1-EGFP mice compared to AD-EGFP mice (88.47 ± 6.28 vs. 107.17 ± 4.63 , $P=0.034$, $n=7$, Figure 5J, K). To determine the effectiveness of intracerebroventricular injection, brain slices (30 μ m) from the three groups were washed with PBS (three times, 5 min each time) and sealed with an anti-fluorescence quenching sealing solution containing DAPI for confocal laser scanning. Results showed that the AAVs carrying EGFP in each group were mainly distributed in the hippocampus (Figure 5L), strongly suggesting successful microinjection into the lateral ventricle. Collectively, our results indicate that SIL1 overexpression significantly suppressed APP amyloidogenic processing.

DISCUSSION

Studies have shown that SIL1 is highly expressed in the hippocampus and is closely associated with neurodevelopment, memory, and learning (Inaguma et al., 2014; Xu et al., 2019). Moreover, SIL1 has been shown to play a protective role in AD. In this study, SIL1 expression was significantly decreased in the brains of APP23/PS45 mice,

suggesting its potential involvement in the pathogenesis of AD, although the mechanism remains unclear. To investigate the role of SIL1 in APP processing, we overexpressed SIL1-myc in N2A^{APP} and 2EB2 cells, resulting in a significant decrease in the protein levels of APP, PS1, C99, and C89, while the protein level of BACE1 remained unchanged. Conversely, SIL1 knockdown in 2EB2 cells not only reversed the protein levels of APP, PS1, C99, and C89, but also increased the protein level of BACE1. These findings imply that the effects of overexpression and knockdown were not completely opposite. Notably, endogenous SIL1 may not directly interact with BACE1, as introducing exogenous SIL1 into the cells did not result in a significant change in BACE1 levels. Furthermore, we microinjected AAV carrying SIL1 into the lateral ventricles of APP23/PS45 mice. This elevation of SIL1 significantly reduced the APP processing and A β deposition and improved both short-term and long-term spatial memory based on the Y-maze and MWM tests, respectively. Collectively, these findings suggest that SIL1 plays a protective role in APP23/PS45 mice by decreasing APP processing and A β deposition.

AD is characterized by the accumulation of A β in the brain with hyperphosphorylated microtubule-associated tau. Previous studies assessing genetic, biochemical, and behavioral components suggest that the generation of neurotoxic A β from sequential APP proteolysis is a crucial step in AD development (Boerwinkle et al., 2023; Elangovan et al., 2023; Masters et al., 2015; O'Brien & Wong, 2011; Selkoe & Hardy, 2016). Chaperone-mediated autophagy (Bourdenx et al., 2021; Zhang et al., 2023a) plays an important role in AD pathogenesis by regulating A β and tau metabolism. However, the impact of SIL1, a co-chaperone, on APP processing related to autophagy remains unclear. In this study, we observed a significant increase in APP mRNA expression after SIL1 knockdown in 2EB2 cells. However, the degradation rates of APP protein and mRNA were not significantly altered, as shown by WB analysis and quantitative PCR, implying that SIL1 decreases APP processing by reducing APP transcription under pathological conditions. Consequently, the reduction in APP expression levels leads to decreased APP processing. However, further studies are required to fully elucidate the mechanism by which SIL1 affects APP mRNA expression.

Recent studies have shown that SIL1 may function as an oncogene, showing up-regulation in certain types of cancer, such as breast cancer (Li et al., 2020) and glioblastoma multiforme (Xu et al., 2018). SIL1 suppression has been found to inhibit cancer cell proliferation and induce apoptosis by activating caspase-3/7 or inhibiting the AKT-mTOR pathway. These findings raise concerns regarding the safety of SIL1 overexpression. However, in the context of AD, SIL1 may play a beneficial role in reducing neuronal loss and synaptic impairment, thereby improving cognitive function in APP23/PS45 mice. Previous research has shown that SIL1 primarily accumulates in the postsynaptic density (PSD) fraction of neurons and directly interacts with proteins such as GluN2A. Moreover, SIL1 knockdown results in the inactivation of Reelin signaling and impedes synaptic NMDA receptor maturation in young mice at 3 weeks of age (Xu et al., 2019). Nevertheless, the specific mechanism of action of SIL1 in adult APP23/PS45 mice remains unknown. A recent report highlighted the involvement of many genes in synaptic plasticity in AD (Wang et al., 2023), suggesting that further

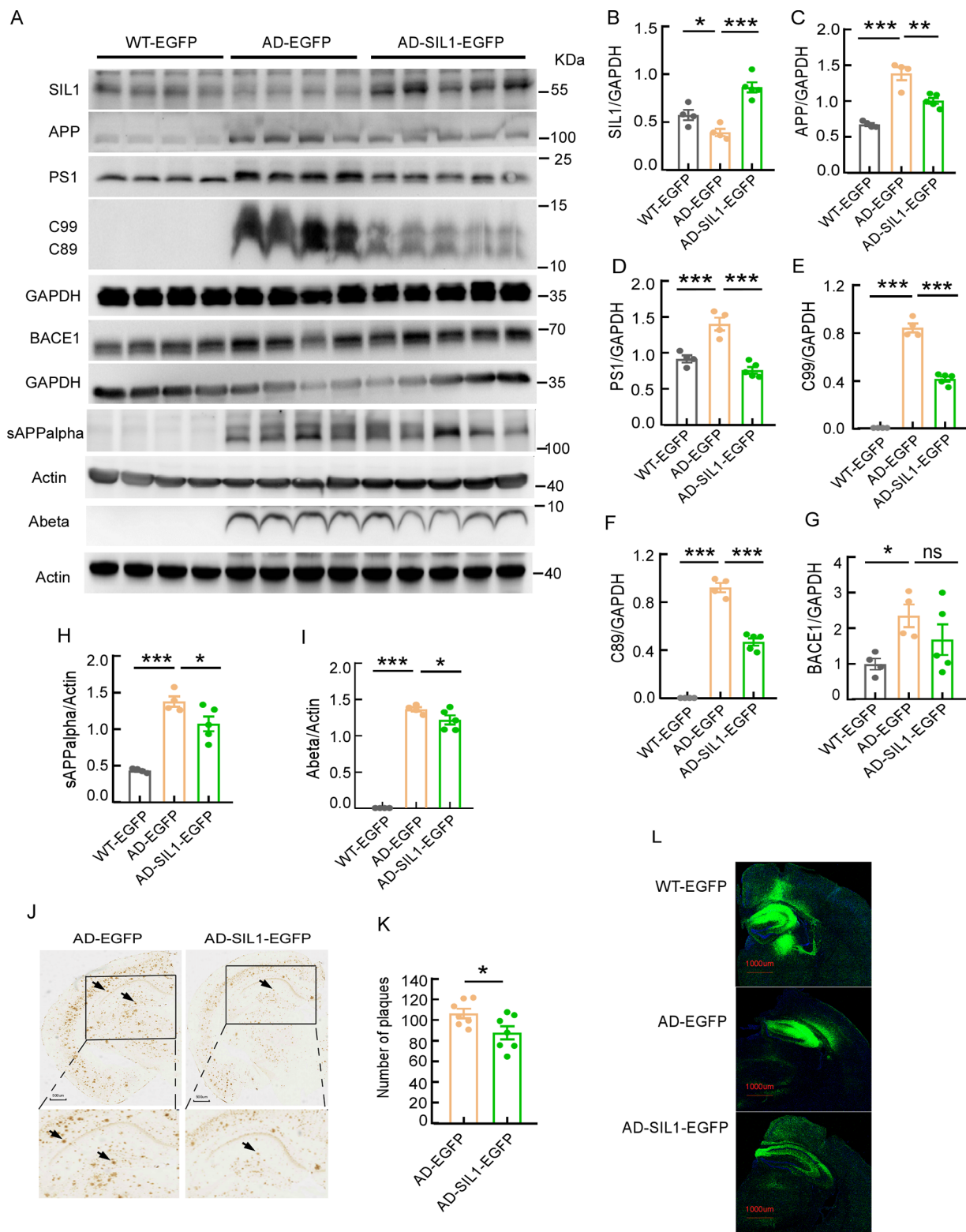


Figure 5 Overexpression of SIL1 significantly reduced APP processing and number of plaques in APP23/PS45 mice

SIL1 decreased APP processing *in vivo*. All mice were sacrificed, with half the hippocampus extracted for WB analysis after behavioral experiments. A: Protein levels of SIL1, APP, PS1, C99, C89, sAPP α , A β , and BACE1 were detected by WB among WT-EGFP (WT mice microinjected with negative-control AAV), AD-EGFP (APP23/PS45 mice microinjected with negative-control AAV), and AD-SIL1-EGFP mice (APP23/PS45 mice microinjected with SIL1-overexpression AAV). $n=4-5$ mice in each group (WT-EGFP, $n=4$; AD-EGFP, $n=4$; AD-SIL1-EGFP, $n=5$). Qualification of B: SIL1, C: APP, D: PS1, E: C99, F: C89, G: BACE1, H: sAPP α , and I: A β , with protein levels normalized to their corresponding GAPDH or actin levels for comparison. L: Immunofluorescent staining showed distribution of AAVs carrying EGFP distributed in the hippocampus of mice in three groups. Scale bar: 1 000 μ m. J: Plaques in AD-SIL1-EGFP and AD-EGFP groups by immunohistochemical staining. Scale bar: 500 μ m. K: Quantification of plaques between AD-EGFP and AD-SIL1-EGFP mice. $n=7$ animals in each group. Data are presented as mean \pm SEM. P -values were determined by one-way ANOVA with Dunnett's *post hoc* analysis. ns: Not significant; *: $P<0.05$; **: $P<0.01$; ***: $P<0.001$.

research is needed to determine whether SIL1 cooperates with these genes to influence AD progression. Furthermore, APP23/PS45 mice exhibit early-onset familial AD, which accounts for less than one percent of AD cases in human patients (Chen & Zhang, 2022). Thus, focusing solely on SIL1 in this model may present limitations. Whether SIL1 levels decrease in AD patients and contribute to A β clearance rather than its generation requires further study.

In conclusion, this study demonstrated that SIL1 levels were decreased in APP23/PS45 mice and that its overexpression improved cognitive impairment by inhibiting APP amyloidogenic processing to reduce A β deposition. These findings suggest that SIL1 may be a potential therapeutic target for AD. However, additional research is required to elucidate the mechanisms by which SIL1 influences APP processing and to evaluate its safety in therapeutic applications.

DATA AVAILABILITY

The raw RNA-seq data reported in this study are available from the NCBI database (BioProjectID PRJNA1099875), China National Center for Bioinformatics database (GSA-Human: HRA005214), and Science Data Bank database (DOI: 10.57760/sciencedb.j00139.00131).

COMPETING INTERESTS

The authors declare that they have no competing interests.

AUTHORS' CONTRIBUTIONS

Q.W. and W.S. conceived and designed the research. Q.W., Y.J., Z.M., X.D., D.H., and L.J. conducted the experiments. W.Z. and W.S. contributed reagents, materials, and analytical tools. W.S. and W.Z. supervised the project. Q.W., W.Z., and W.S. wrote the manuscript and revised manuscript. All authors read and approved the final version of the manuscript.

REFERENCES

Anttonen AK, Mahjneh I, Hämäläinen RH, et al. 2005. The gene disrupted in Marinesco-Sjögren syndrome encodes SIL1, an HSPA5 cochaperone. *Nature Genetics*, **37**(12): 1309–1311.

Bayer TA, Cappai R, Masters CL, et al. 1999. It all sticks together—the APP-related family of proteins and Alzheimer's disease. *Molecular Psychiatry*, **4**(6): 524–528.

Boerwinkle AH, Gordon BA, Wisch J, et al. 2023. Comparison of amyloid burden in individuals with down syndrome versus autosomal dominant Alzheimer's disease: a cross-sectional study. *The Lancet Neurology*, **22**(1): 55–65.

Bourdenx M, Martín-Segura A, Scrivo A, et al. 2021. Chaperone-mediated autophagy prevents collapse of the neuronal metastable proteome. *Cell*, **184**(10): 2696–2714. e25.

Bromley-Brits K, Deng Y, Song WH. 2011. Morris water maze test for learning and memory deficits in Alzheimer's disease model mice. *Journal of Visualized Experiments*, (53): 2920.

Chen ZY, Zhang Y. 2022. Animal models of Alzheimer's disease: applications, evaluation, and perspectives. *Zoological Research*, **43**(6): 1026–1040.

Chung KT, Shen Y, Hendershot LM. 2002. BAP, a mammalian BiP-associated protein, is a nucleotide exchange factor that regulates the ATPase activity of BiP. *Journal of Biological Chemistry*, **277**(49): 47557–47563.

Deng Y, Wang Z, Wang RT, et al. 2013. Amyloid- β protein (A β) Glu11 is the major β -secretase site of β -site amyloid- β precursor protein-cleaving enzyme 1 (BACE1), and shifting the cleavage site to A β Asp1 contributes to Alzheimer pathogenesis. *European Journal of Neuroscience*, **37**(12): 1962–1969.

Du YH, Du YX, Zhang Y, et al. 2019. MKP-1 reduces A β generation and alleviates cognitive impairments in Alzheimer's disease models. *Signal Transduction and Targeted Therapy*, **4**: 58.

Elangovan A, Babu HWS, Iyer M, et al. 2023. Untangle the mystery behind DS-associated AD - Is APP the main protagonist?. *Ageing Research Reviews*, **87**: 101930.

Esch FS, Keim PS, Beattie EC, et al. 1990. Cleavage of amyloid β peptide during constitutive processing of its precursor. *Science*, **248**(4959): 1122–1124.

Filézac De L'Etang A, Maharjan N, Cordeiro Braña M, et al. 2015. Marinesco-Sjögren syndrome protein SIL1 regulates motor neuron subtype-selective ER stress in ALS. *Nature Neuroscience*, **18**(2): 227–238.

Inaguma Y, Hamada N, Tabata H, et al. 2014. *SIL1*, a causative cochaperone gene of Marinesco-Sjögren syndrome, plays an essential role in establishing the architecture of the developing cerebral cortex. *EMBO Molecular Medicine*, **6**(3): 414–429.

Karran E, De Strooper B. 2022. The amyloid hypothesis in Alzheimer disease: new insights from new therapeutics. *Nature Reviews Drug Discovery*, **21**(4): 306–318.

Kraeuter AK, Guest PC, Samyai Z. 2019. The Y-maze for assessment of spatial working and reference memory in mice. In: Guest OC. Pre-Clinical Models: Techniques and Protocols. New York: Humana, 105–111.

Labisch T, Buchkremer S, Phan V, et al. 2018. Tracking effects of SIL1 increase: taking a closer look beyond the consequences of elevated expression level. *Molecular Neurobiology*, **55**(3): 2524–2546.

Li ZF, Xu WW, Li JD, et al. 2020. Nucleotide exchange factor SIL1 promotes the progress of breast cancer cells via regulating the cell cycle and apoptosis. *Science Progress*, **103**(1): 36850419891046.

Liao XX, Cai F, Sun ZF, et al. 2020. Identification of Alzheimer's disease-associated rare coding variants in the *ECE2* gene. *JCI Insight*, **5**(4): e135119.

Liu X, Che RB, Liang WP, et al. 2022. Clusterin transduces Alzheimer-risk signals to amyloidogenesis. *Signal Transduction and Targeted Therapy*, **7**(1): 325.

Liu ZC, Chu J, Lin L, et al. 2016. SIL1 rescued bip elevation-related tau hyperphosphorylation in ER stress. *Molecular Neurobiology*, **53**(2): 983–994.

Ly PTT, Wu YL, Zou HY, et al. 2013. Inhibition of GSK3 β -mediated BACE1 expression reduces Alzheimer-associated phenotypes. *The Journal of Clinical Investigation*, **123**(1): 224–235.

Masters CL, Bateman R, Blennow K, et al. 2015. Alzheimer's disease. *Nature Reviews Disease Primers*, **1**: 15056.

O'Brien RJ, Wong PC. 2011. Amyloid precursor protein processing and Alzheimer's disease. *Annual Review of Neuroscience*, **34**: 185–204.

Peng L, Bestard-Lorigados I, Song W. 2022. The synapse as a treatment avenue for Alzheimer's disease. *Molecular Psychiatry*, **27**(7): 2940–2949.

Rosam M, Krader D, Nickels C, et al. 2018. Bap (Sil1) regulates the molecular chaperone BiP by coupling release of nucleotide and substrate. *Nature Structural & Molecular Biology*, **25**(1): 90–100.

Selkoe DJ, Hardy J. 2016. The amyloid hypothesis of Alzheimer's disease at 25 years. *EMBO Molecular Medicine*, **8**(6): 595–608.

Senderek J, Krieger M, Stendel C, et al. 2005. Mutations in *SIL1* cause Marinesco-Sjögren syndrome, a cerebellar ataxia with cataract and myopathy. *Nature Genetics*, **37**(12): 1312–1314.

Sun XL, Wang YC, Qing H, et al. 2005. Distinct transcriptional regulation and function of the human *BACE2* and *BACE1* genes. *The FASEB Journal*, **19**(7): 739–749.

Wang T, Zhou YQ, Wang Y, et al. 2023. Long-term potentiation-based screening identifies neuronal PYGM as a synaptic plasticity regulator participating in Alzheimer's disease. *Zoological Research*, **44**(5): 867–881.

Wang Z, Xu Q, Cai F, et al. 2019. BACE2, a conditional β -secretase,

- contributes to Alzheimer's disease pathogenesis. *JCI Insight*, **4**(1): e123431.
- Xu H, Xu SC, Zhang R, et al. 2018. SIL1 functions as an oncogene in glioma by AKT/mTOR signaling pathway. *OncoTargets and Therapy*, **11**: 3775–3783.
- Xu SL, Zhu J, Mi K, et al. 2019. Functional role of SIL1 in neurodevelopment and learning. *Neural Plasticity*, **2019**: 9653024.
- Zhang ST, Cai F, Wu YL, et al. 2020. A presenilin-1 mutation causes Alzheimer disease without affecting Notch signaling. *Molecular Psychiatry*, **25**(3): 603–613.
- Zhang ST, Wang Z, Cai F, et al. 2017. BACE1 cleavage site selection critical for amyloidogenesis and Alzheimer's pathogenesis. *Journal of Neuroscience*, **37**(29): 6915–6925.
- Zhang XW, Zhu XX, Tang DS, et al. 2023a. Targeting autophagy in Alzheimer's disease: Animal models and mechanisms. *Zoological Research*, **44**(6): 1132–1145.
- Zhang Y, Chen HQ, Li R, et al. 2023b. Amyloid β -based therapy for Alzheimer's disease: challenges, successes and future. *Signal Transduction and Targeted Therapy*, **8**(1): 248.
- Zheng QY, Song BB, Li GL, et al. 2022. USP25 inhibition ameliorates Alzheimer's pathology through the regulation of APP processing and A β generation. *The Journal of Clinical Investigation*, **132**(5): e152170.